energies

MDPI

Article

Experimental, Kinetic Modeling and Morphologic Study of the Premixed Combustion of Hydrogen/Methane Mixtures

Miriam Reyes *, Rosaura Sastre, Blanca Giménez and Clara Sesma

Department of Energy and Fluid-Mechanics Engineering, University of Valladolid, Paseo del Cauce, 59, E-47011 Valladolid, Spain; rosaura.sastre@uva.es (R.S.); blagim@eii.uva.es (B.G.); csmangu@gmail.com (C.S.)
* Correspondence: miriam.reyes@uva.es

Abstract: In this work, an experimental study and kinetic characterization of the combustion process and a morphologic study of hydrogen/methane–air mixtures are presented. The experimental study was performed in an optical access cylindrical constant-volume combustion bomb. This bomb is equipped to register the instantaneous pressure during combustion and records the combustion images using the high-speed Schlieren optical technique. This provides straightforward information to compute the flame propagation speed and direct evidence of the apparition of cellularity on the flame front. Through the images of the combustion process, it is possible to conduct a morphological study of the process using a flame monitoring model. Simultaneously, by means of a two-zone thermodynamical model, with the temporal evolution of pressure as the main intake, significant parameters are determined during the combustion process of different fuels under premixed conditions: burning velocity, rate of combustion, burned and unburned temperature, burned mass fraction, and rate of heat release, among others. Experimental results are compared with kinetic modeling results obtained with the Cantera package using the Gri-Mech 3.0 kinetic mechanism. Results show that a greater percentage of hydrogen in the fuel mixture increases the burning velocity and the cellularity of the flame front surface. At the same time, leaner mixtures and higher equivalence ratios enhance the apparition of the cellularity onset in the flames. Burning velocity increases with the increase in the initial temperature and the fuel/air mixture equivalence ratio. All the results obtained were validated with other data from the literature.

Keywords: hydrogen; methane; combustion bomb; laminar burning velocity; cellularity

Citation: Reyes, M.; Sastre, R.; Giménez, B.; Sesma, C. Experimental, Kinetic Modeling and Morphologic Study of the Premixed Combustion of Hydrogen/Methane Mixtures. *Energies* **2022**, *15*, 3722. https://doi.org/10.3390/en15103722

Academic Editor: Venera Giurcan

Received: 25 April 2022
Accepted: 17 May 2022
Published: 19 May 2022

1. Introduction

Fossil fuels are the basis of current industry because they are extensively used in all areas of daily life, making them an important aspect of the global economy. Nevertheless, the limitation on fossil fuel resources leads to their depletion, increasing oil prices and the energy dependence of fossil fuel-producing countries. In addition, the combustion of fossil fuels has a negative effect on the environment and on people's health. Altogether, this makes it necessary to look for new cleaner energy sources and new fuels, in addition to increasing the combustion process efficiency. One possible solution to the above problem is the development and use of alternative fuels with a renewable origin.

Gaseous fuels have advantages over liquids and solids, as their polluting emissions can be more easily controlled, achieving greater efficiencies. They produce lower CO or CO_2 emissions because they have a high hydrogen/carbon ratio [1]. However, gaseous fuels have disadvantages due to their low energy density per unit volume or per unit mass, which is lower than that of liquid fuels. Therefore, the storage system requires more space, and this leads to a diminution of the autonomy, since vehicle tanks have a volume limitation. Natural gas (NG) and hydrogen are some of the most interesting alternative or residual gaseous fuels.

The laminar burning velocity (LBV) is one of the main parameters in engine modelling; it is used in predictive and diagnosis models to understand the combustion process taking place in an internal combustion engine, as well as for diagnosis and predictive models of this engine [2,3]. In addition, computational fluid dynamics models are needed to design new engines, simulate hydrogen/methane combustion in internal combustion engines, and predict the optimal design. These models need chemical kinetics and LBV results.

Many previous studies on combustion processes focused on the study of methane/air flames [4–9] and/or hydrogen/air flames [10–13]. Various experimental studies focused on measuring laminar burning velocity in methane/hydrogen/air blends [7,14–17]. Scholte and Vaags [18] were the pioneers in measuring the speed of this mixture using the tube burner method. Liu et al. [19] and Huang et al. [20] conducted more extensive experimental studies on a wide range of relative doses and hydrogen fraction/content in methane–hydrogen/air flames. Other investigations focused on the study of instabilities developed in the flame [21,22] during the combustion process [23–25] which, in some cases, leads to a cellular flame front. Phenomena that can produce instabilities in the flame front (in a laminar regime) of a premixed combustion are volume forces, hydrodynamic effects, and thermo-diffusive effects [26,27]. An unstable structure increases the burning velocity [28–30]. The understanding of hydrogen/methane combustion and cellularity in flames is necessary for improving the performance of internal combustion engines.

Studies can be classified into two categories: the first is from the point of view of improving the methane flame by adding hydrogen; the second is from the point of view of hydrogen flame inhibition by adding methane. Yu et al. [7] studied the characteristics of the laminar combustion rate of methane/hydrogen/air flames and observed a linear correlation between the laminar burning velocity of the fuel mixture and the hydrogen content. Law and Kwon [16] investigated the possibility of adding hydrocarbons to hydrogen flames to reduce the risk of explosion and found that adding a small methane content could significantly decrease the laminar burning velocity and retard the apparition of instabilities on the hydrogen/air flames (with a thermal–diffusive or hydrodynamic origin).

The addition of hydrogen to methane increases the H/C ratio, which leads to a reduction in the CO, HC, and CO_2 emissions. However, increasing the percentage of hydrogen increases the flame temperature and NOx emissions [3,31–35]. Jiang et al. [36] investigated in a combustion chamber the relationship between the cellular structure of a flame front and the pressure of methane/hydrogen/air mixtures under laminar premixed flame conditions for different equivalence ratios and percentages of hydrogen. Kim et al. [37] conducted an experimental investigation about the onset of cellular instabilities and the acceleration of the flame. Wu et al. [38] conducted an experimental investigation to study the self-acceleration of hydrogen flames under cellular conditions. Tinaut et al. [24] characterized hydrogen flames morphology under cellularity conditions using a parameter to quantify the cellularity in the flame. Di Sarli et al. [39] investigated the laminar burning velocities of hydrogen/methane/air mixtures using a kinetic mechanism varying the equivalence ratio and fuel composition. El-Sherif [40] proposed the control of emissions by adding hydrogen to methane flames, studied hydrogen/methane flames using a kinetic mechanism, and obtained correlations.

This paper focuses on the study of hydrogen/methane/air combustion in a cylindrical constant-volume combustion bomb analyzing the laminar burning velocity and morphology of the fuel mixtures. For this goal, three concurrent methodologies are employed: temporal pressure register (examined with a two-zone diagnosis model), radius evolution obtained from the flame development recorded with the Schlieren technique, and kinetic modeling. In addition, a morphological study of the hydrogen/methane/air blends is presented, and flame front thickness is studied. Finally, experimental results are also compared with kinetic modeling results using Cantera in terms of laminar burning velocity and NOx, CO, and CO_2 emissions with the increase in hydrogen in the fuel mixture.

2. Experimental Specifications

Laminar burning velocity of the premixed gas was measured in a cylindrical constant-volume combustion bomb with a diameter of 114 mm and a height of 135 mm, a high-speed image system, and an ignition system (Figure 1). Through this facility, it is possible to observe the flame development and the flame front morphology. For each experiment, the combustion chamber was vacuumed and filled with hydrogen/methane/air mixtures according to the corresponding partial pressure. After that, the mixture was ignited at the center of this chamber by two electrodes. The flame propagation was filmed using the Schlieren technique with a high-speed camera Phantom V210 at 7000 frames per second.

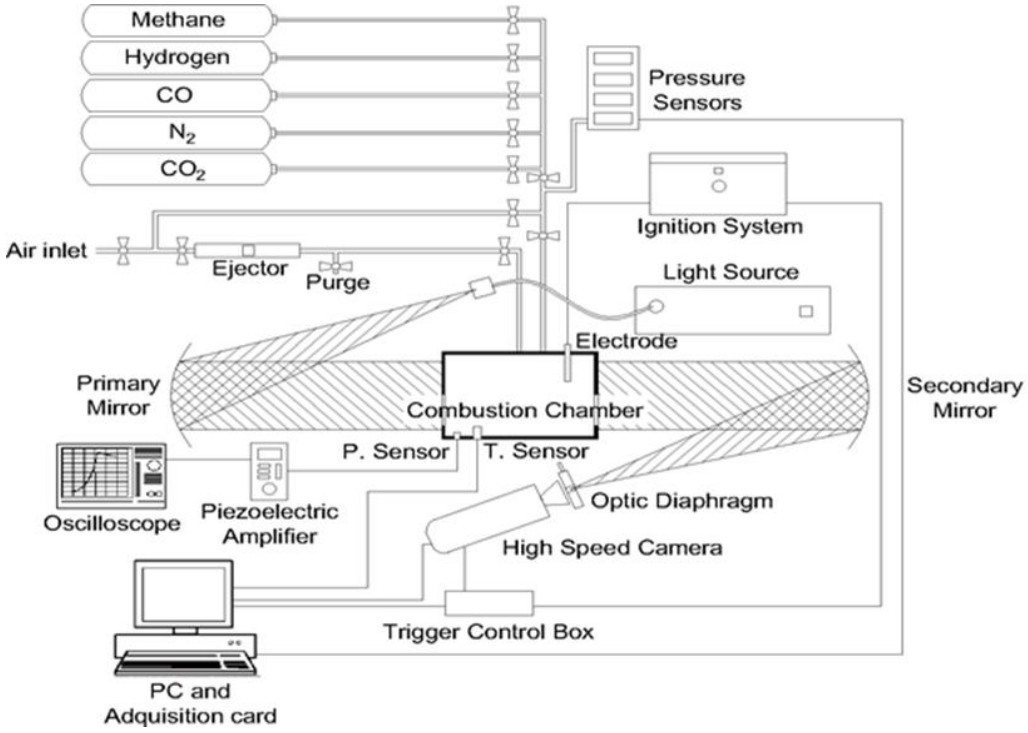

Figure 1. Scheme of the experimental setup.

A mathematical algorithm was built for the processing of the images obtained with the optical assembly. Pressure was recorded, during the combustion process, using a piezoelectric pressure transducer (model Kistler type 7063). The complete components of the experimental installation, the methodology used in this research, and a full description of the algorithm for image processing were detailed in a previous study [24].

Characterization of cellularity regimes includes items such as the identification of the conditions of the instability's onset, which depends on the main operating conditions: pressure, temperature, and equivalence ratio. A detailed description of the experimental installation was presented in previous studies [24,41].

3. Results

In this section, results obtained from the experiments of hydrogen/methane–air mixtures are presented. The experiments were performed for different fuel/air mixtures, varying the percentage of hydrogen in the mixture from 0% to 100% and the equivalence ratio from 0.5 to 1.0. Initial pressure and temperature were fixed at 0.1 MPa and 315 K for all experiments. Lean fuel/air mixtures were chosen as the region of interest in spark ignition engines, and different mixtures of hydrogen and methane were used to determine the influence of the hydrogen addition on the methane combustion.

3.1. Laminar Burning Velocity Results

The results presented of the laminar burning velocity were obtained using three different methodologies: firstly, from the diagnosis of the instantaneous pressure inside the combustion chamber, u_l^p (with the two-zone thermodynamical model); secondly, from the recording of the combustion images, u_l; thirdly, using Cantera software with a kinetic mechanism, LBV. In the three cases, the influence of the hydrogen content and the fuel/air equivalence ratio was investigated. Results obtained with different methods were compared among themselves and with the available literature to check the dispersion of the results. Finally, a morphological study of the hydrogen/methane flames was performed.

3.1.1. Laminar Burning Velocity from the Pressure Register

Initially, the laminar burning velocity was obtained from the temporal pressure registered during the combustion with a two-zone thermodynamic model, in which the combustion chamber was divided into two zones: burned and unburned; more details of the model can be obtained in Tinaut et al. [24]. The burned mass fraction was evaluated from the pressure register by means the thermodynamic model, detailed in Reyes et al. [9]. The laminar burning velocity u_l^p was calculated from the mass burning rate $\dot{m}_b$, the unburned mixture density ρ_u, and the flame front surface A_f, according to the following expression:

$$u_l^p = \frac{\dot{m}_b}{\rho_u \cdot A_f}. \quad (1)$$

In Figures 2 and 3, curves of the evolution of the pressure inside the combustion bomb versus the combustion time and curves of the laminar burning velocity (u_l^p) versus the temperature of the unburned zone are presented.

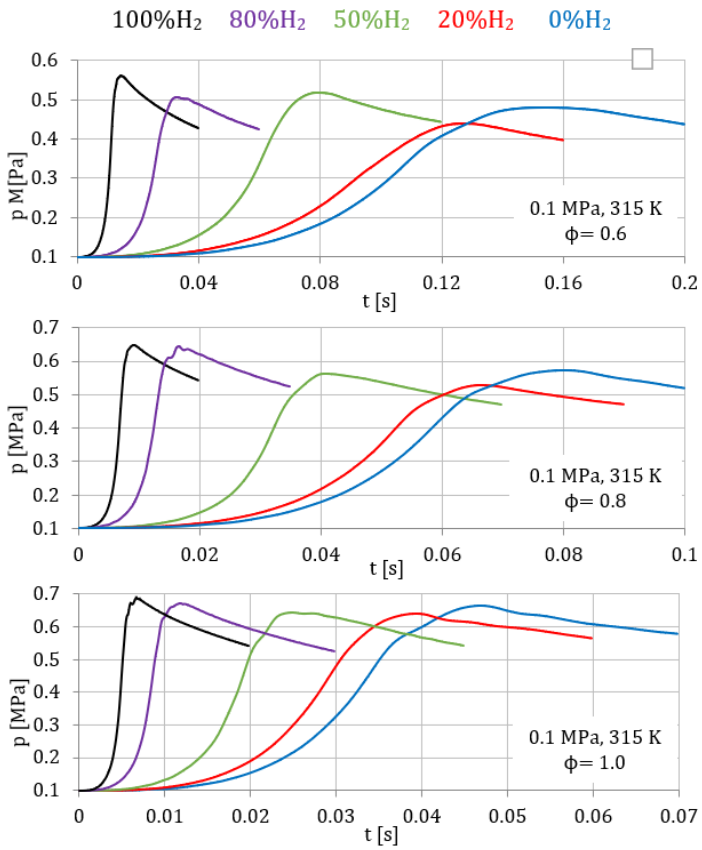

Figure 2. Temporal evolution of pressure for fuel/air mixtures with different percentage of hydrogen, 0.1 MPa, 315 K, and equivalence ratios of 0.6, 0.8, and 1.

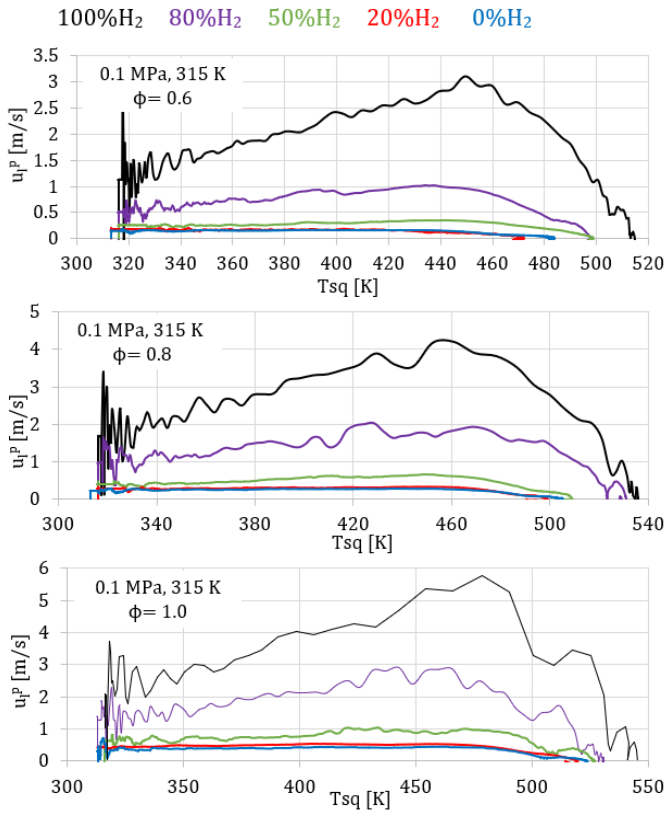

Figure 3. Laminar burning velocity for fuel/air mixtures with different percentage of hydrogen, 0.1 MPa, 315 K and equivalence ratios of 0.6, 0.8, 1.

Figure 2 presents the temporal evolution of pressure for mixtures with different percentages of hydrogen (from 0% to 100%) and with different equivalence ratios (0.6, 0.8, and 1.0), all for constant initial pressure (0.1 MPa) and temperature (315 K). It is possible to see that hydrogen enhanced the combustion process, reaching the peak pressure earlier, for all the equivalence ratios tested. Accordingly, Figure 3 shows the corresponding burning velocities obtained with the thermodynamic model, where it is possible to see the increment in the laminar burning velocity with the percentage of hydrogen in the fuel mixture. The percentage of hydrogen increased the H concentration produced during the combustion, increasing the burning velocity of the fuel/air mixture.

Results of the laminar burning velocities for different fuel mixtures (percentage of hydrogen) and various equivalence ratios (from 0.5 to 1.0) are presented in Figure 4, for 0.1 MPa and 315 K initial conditions. As shown in Section 1, the behaviors of hydrogen and methane are very different; depending on the amount of hydrogen added to the mixture, the behavior will be close to that of hydrogen (known as a dominant hydrogen mixture) or to that of methane (a dominant methane mixture). The transitional regime was obtained in this work for percentages of hydrogen in the fuel mixture higher than 30% and lower than 80%. This regime was characterized by the laminar burning velocity increasing exponentially with the hydrogen content in the fuel mixture. When the percentage of hydrogen in the fuel mixture was lower than 30%, methane dominated the combustion process, and the laminar burning velocity increased linearly with the hydrogen content. On the other hand, when the percentage of hydrogen exceeded 80%, the combustion was dominated by hydrogen dominated and the laminar burning velocity increased linearly, but with a higher slope than in the methane-dominated regime. Other studies obtained similar tendencies; for example, Di Sarli et al. [39] divided the hydrogen/methane combustion into three regimes according to the degree to which the hydrogen content affects the laminar burning velocity of the fuel mixture: methane-dominated combustion ($X_{H2} < 0.5$) where the laminar burning velocity increases linearly with the hydrogen content, the transition regime ($0.5 \leq X_{H2} \leq 0.9$)

where the laminar burning velocity increases exponentially with the hydrogen content, and hydrogen-dominated combustion(X_{H2} > 0.9) where the laminar burning velocity increases linearly with the hydrogen content. In addition, in all tested mixtures, the equivalence ratio enhanced the laminar burning velocity, due to the improvement of the reaction activity.

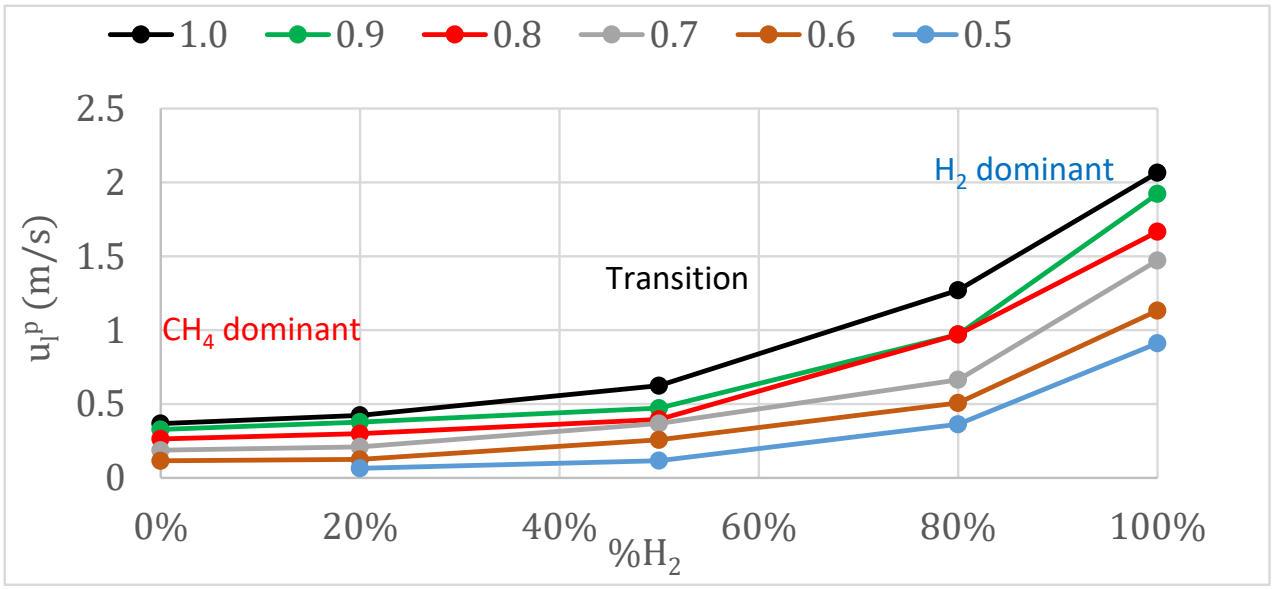

Figure 4. Laminar burning velocity, obtained with pressure register, versus the percentage of hydrogen in the fuel/air mixture, with initial conditions of 0.1 MPa and 315 K.

3.1.2. Laminar Burning Velocity Obtained from Schlieren Images (u_l)

The premixed combustion, originating at the center of the combustion bomb, propagates spherically with the flame propagation speed $S_n = {}^{dr_u}/_{dt}$, where r_u is the flame radius obtained as a correction of the instantaneous radius observed by Schlieren images (r_{sch}) [4,42], shown in Equation (1), where ρ_u and ρ_b are the unburned and burned densities, respectively, and δ_l is the laminar flame thickness given by $\delta_l = {}^{\nu}/_{u_l}$, in which u_l is the laminar burning velocity estimated using r_{sch}, and ν is the kinematic viscosity of the unburned mixture.

$$r_u = r_{sch} + 1.95 \cdot \delta_l \cdot \rho_u \cdot \rho_b^{0.5}. \quad (2)$$

The stretched laminar burning velocity, u_n, can be obtained from the propagation speed ($u_n = {}^{\rho_b}/_{\rho_u} S_n$) using the thermal expansion coefficient ($\sigma = {}^{\rho_u}/_{\rho_b}$) [43].

The expanding rate of a spherically expanding flame due to the flame front curvature [4] is the flame stretch rate: $\alpha = \frac{1}{A_f} \cdot \frac{dA_f}{dt} = \frac{2}{r} S_n$, where A_f is the flame front area.

The laminar burning velocity is affected by the flame stretch because of the coupling between diffusion and hydrodynamics caused by the change in the velocity of the gas flow due to the gas expansion. The relationship between the stretched and unstretched laminar burning velocity is as follows: $u_n - u_l = -L_b \alpha$, where L_b is the Markstein length and u_l is the unstretched laminar burning velocity [44]. The stretch influence can be eliminated from the flame propagation speed, obtaining the unstretched flame propagation speed, S_l, extrapolating the flame propagation speeds for a stretch of zero (see Figure 5), and obtaining the laminar burning velocity from $u_l = {}^{\rho_b}/_{\rho_u} S_l$.

Figure 5 shows the flame propagation speed, *Sn*, versus the stretch rate, α, for an 80% H_2/20% CH_4 mixture at ϕ = 0.9. In this figure, the laminar and cellular regimen can be clearly visualized. For high stretch rates (small flame radius), the flame propagation speed was high. As the flame expanded, the speed of the flame slowly dropped due to the decrease in flame stretch rate. As stretch was further reduced, a point was reached where the flame became unstable (critical point) and visible cellularity developed in the flame front, producing an increase in flame propagation speed. The point at which the

flame velocity begins to rapidly accelerate with decreasing stretch defines a critical point. This critical point is associated with a Peclet number, P_{ecr}, given by the flame radius at the start of the flame acceleration, normalized by the flame thickness ($Pe = r/\delta_l$). The unstretched flame velocity, S_l, was calculated as presented in Figure 5, and the values of S_l were determined from a linear fit of Sn against α over the largest possible range of radii, excluding cellular flame regions and those affected by the spark. When the stretch rate cuts the ordinate, i.e., $\alpha = 0$, it gives rise to the value of S_l, Figure 5.

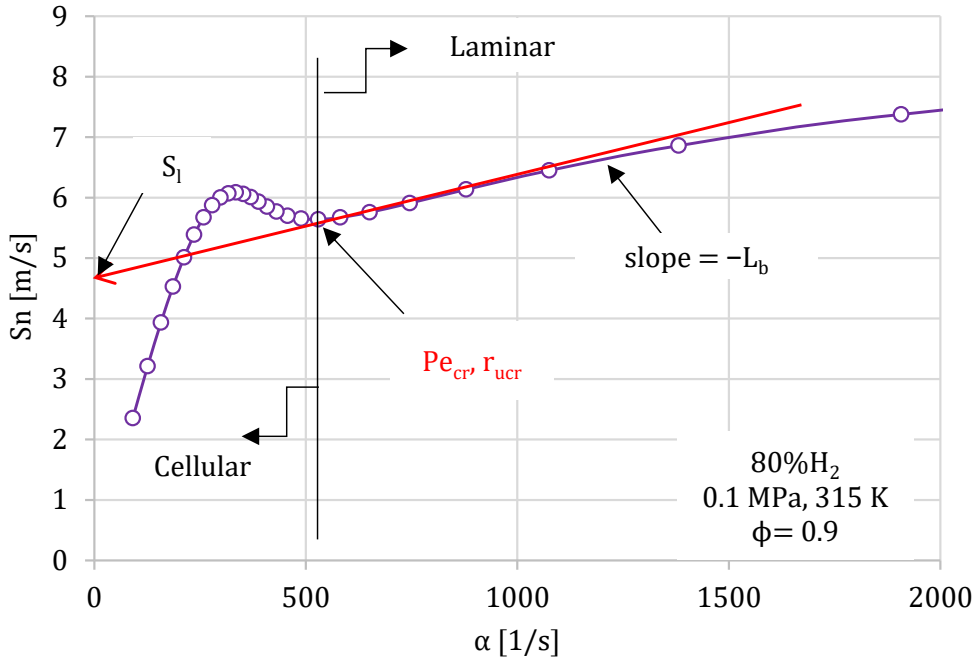

Figure 5. Flame propagation speed versus the stretch rate for 80% H_2/20% CH_4 mixture at initial conditions of ϕ = 0.9, 0.1 MPa, and 315K.

In Figure 6a, the temporal evolution of the flame radius for lean fuel mixtures (for ϕ = 0.8) with different percentages of hydrogen (varying from 0% to 100%) is plotted. At the initial stage of flame development, the flame stretch was big, and the flame stability was strong. With the growth of the flame, the stretch rate of the flame decreased as the flame radius increased. Figure 6a shows that, with increasing hydrogen content in the fuel/air mixture, the slope of the radius evolution increased.

Figure 6b shows the corresponding flame propagation speeds. Here, it is possible to see that the increment in the hydrogen content in the fuel mixture enhanced the combustion process. The unstretched flame propagation speed, S_l, was determined as expressed before the test developed, and the results are presented in Figure 6c.

For hydrogen content less than 50% (dilute hydrogen conditions), the unstretched flame propagation speed represented in Figure 6c increased linearly with the percentage of hydrogen. However, for hydrogen content greater than 50% (hydrogen-rich conditions), the unstretched flame propagation speed increased exponentially with the hydrogen content in the fuel/air mixture.

It can be considered that flame propagates under constant pressure at the beginning of the combustion process, and the variations in the stretched laminar burning velocity can be assigned to stretch rate variations. Figure 6d presents the laminar burning velocity results versus the equivalence ratio for different percentages of hydrogen in the fuel/air mixture from 0% to 100%, where it is possible to see the same upward tendency for the laminar burning velocity. Values of laminar burning velocity for very poor mixtures with low hydrogen content were difficult to obtain using this methodology (0% and 20% of hydrogen and 0.5–0.6 fuel/air equivalence ratio).

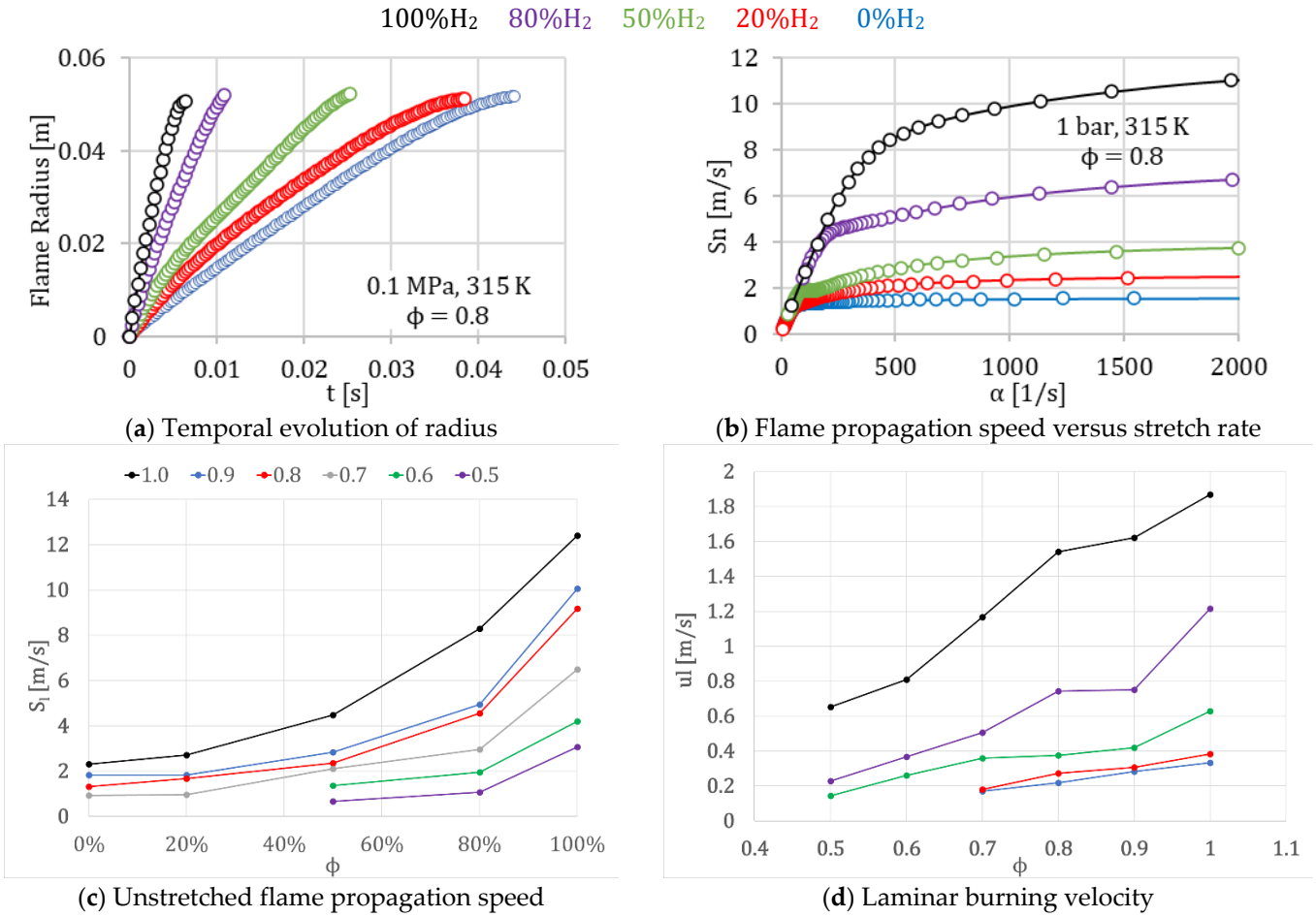

(**a**) Temporal evolution of radius

(**b**) Flame propagation speed versus stretch rate

(**c**) Unstretched flame propagation speed

(**d**) Laminar burning velocity

Figure 6. Radius, flame front propagation speed, unstretched flame propagation speed, and laminar burning velocity of different mixtures of H_2/CH_4, for 1.0 equivalence ratio, obtained using the Schlieren technique.

3.1.3. Laminar Burning Velocity Obtained from Cantera Kinetic Modeling (LBV)

A kinetic study of the combustion process is important to be able to interpret the experimental results; in addition, it improves the understanding of the physical and chemical phenomena that occur during the combustion process. Combustion modeling involves the resolution of a system of differential equations of great computational cost. Currently, there are computational codes that, together with the use of reaction mechanisms, make it possible to find increasingly reliable theoretical solutions to combustion problems. The tool used in this work was CANTERA [45]. The most widely accepted H_2/CH_4/air kinetic reaction mechanisms are GRI-Mech 3.0 [46] and Aramco [12,47–49].

Results of the laminar burning velocity obtained with kinetic modeling using Cantera (denoted as LBV) of fuel/air mixtures obtained using the kinetic mechanisms of GRI-Mech 3.0 and Aramco 1.3 are presented in Figure 7 to study the effect of the addition of H_2. These results show the same tendency for the laminar burning velocity values as that obtained using the other two methodologies. Gri-Mech 3.0 and Aramco results were quite similar for low and medium percentages of hydrogen in the fuel mixture, but differed for mixtures with high hydrogen content, as also seen in other studies [48,50]. The results obtained with the two mechanisms differed for mixtures with high hydrogen contents, due to the complex reactions controlled by the hydrogen sub-model [22]. These two mechanisms have been widely used in modeling the laminar burning velocity of methane and methane/hydrogen mixtures [47,51]. Gri-Mech 3.0 consists of 325 elementary chemical reactions and 53 species, optimized in modeling methane and hydrogen and

tuned for high temperature, whereas Aramco 1.3 consists of 470 chemical reactions and 53 species. Aramco 1.3 predicted higher values of the LBV than Gri-Mech 3.0 for elevated hydrogen contents, despite these mechanisms giving similar values for the other fuel mixtures, with a lower hydrogen fraction. Other authors showed the same differences between the two mechanisms [52] obtaining an overprediction of the constant-volume data in lean conditions.

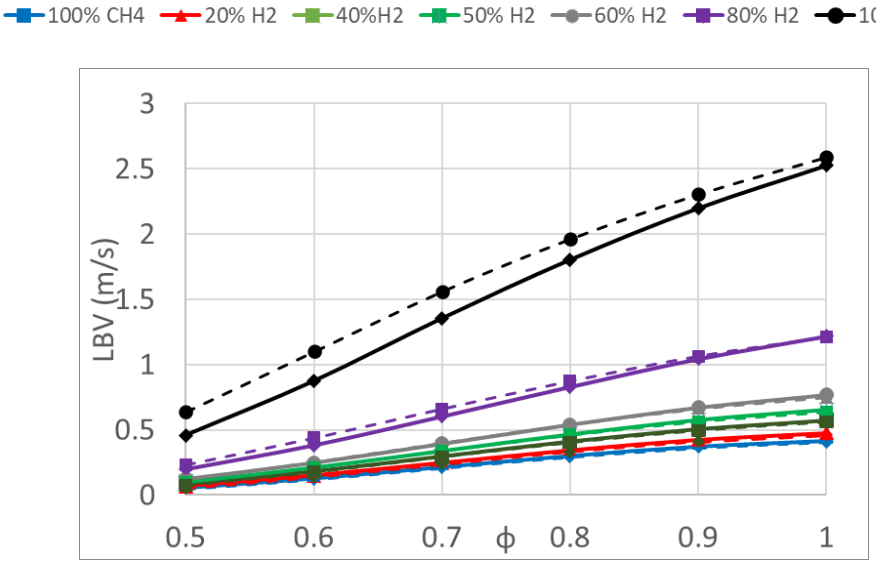

Figure 7. Laminar burning velocity of hydrogen/methane mixtures versus the equivalence ratio obtained with GRI-Mech 3.0 (continuous lines) and Aramco (dashed lines) kinetic mechanisms in conditions of 0.1 MPa and 315 K.

3.2. Laminar Burning Velocity Comparison

In this section, a comparison between laminar burning velocity results obtained with the three different methodologies in this study and with the literature is presented as a function of the fuel/air equivalence ratio, for different percentages of hydrogen in the fuel mixture. The laminar burning velocity of methane/air mixtures at atmospheric pressure and an initial temperature of 300 K is plotted versus the fuel/air equivalence ratio in Figure 8, using some values presented in the review of the laminar burning velocity published by Konnov et al. [53] and in Reyes et al. [14]. Experimental results and predictions of detailed kinetic models (lines) are presented in this plot. The present results are shown in this figure, although the initial temperature is 315 K, obtaining good agreement with the other results. The spherical flame method has been widely used for burning velocity measurements. The big discrepancies in the experimental data presented in Figure 8 could be due to the different measurement techniques. As the spherical flames propagating outward are correlated with the stretch rate, a correction is needed to obtain more accurate burning velocity values; as previously explained, the researchers that used pressure–time data to calculate laminar burning velocity did not take into account the stretching effect.

Results for the laminar burning velocity of different H_2/CH_4 mixtures (20%, 50%, 80%, and 100% H_2) are presented in Figure 9. The *Y*-axis scales are different for each percentage of hydrogen to distinguish curves. In Figure 9, results of the laminar burning velocity for mixtures with 20% hydrogen (blue color) obtained using the three methodologies are presented and compared with those obtained by Hu et al. [54] and by Huang et al. [20]. Results obtained in this investigation agree well with the literature results. It is only possible to see a discrepancy between results obtained with the image method for low equivalence ratios, since those combustions were very slow, and the pressure constant zone used to determine the u_l differed. Data of the laminar burning velocity from the present work together with those from other sources are shown in Figure 9 versus the equivalence ratio

for 50% H_2/50% CH_4, 80% H_2/20% CH_4, and 100% H_2 mixtures (brown, purple, and green colors respectively), obtaining good agreement with the rest of the data.

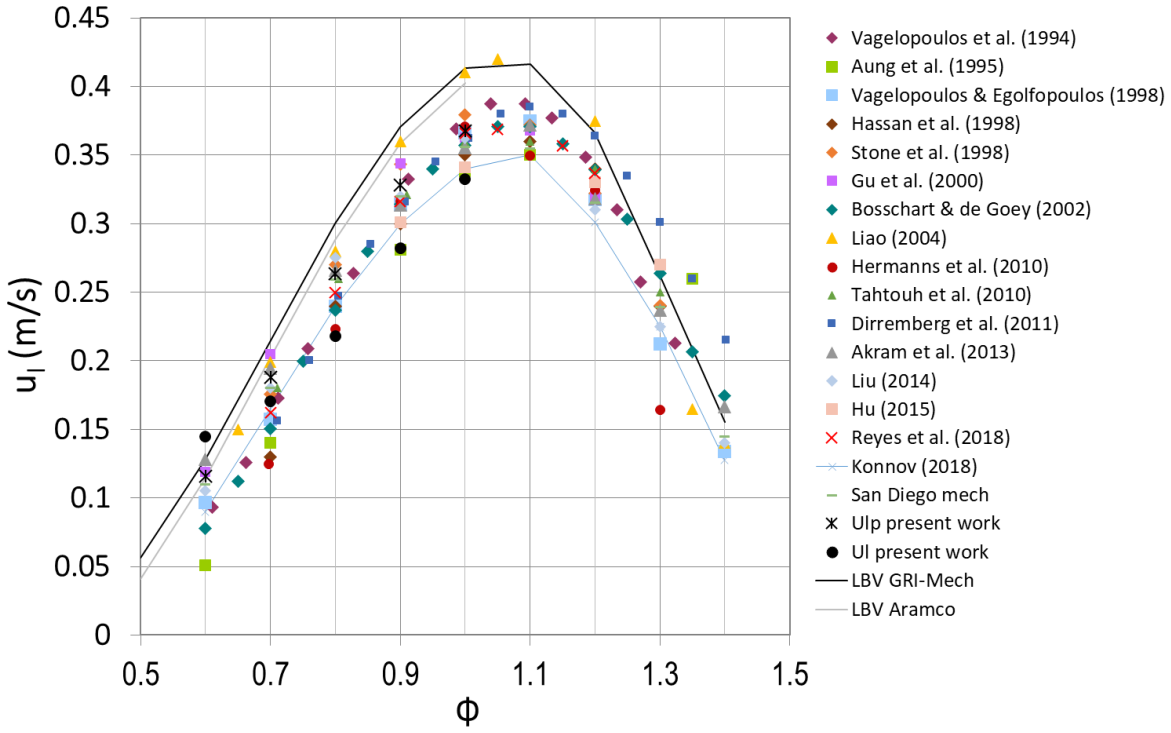

Figure 8. Laminar burning velocity of methane/air in standard conditions obtained in the present work with different methods and compared with the literature results.

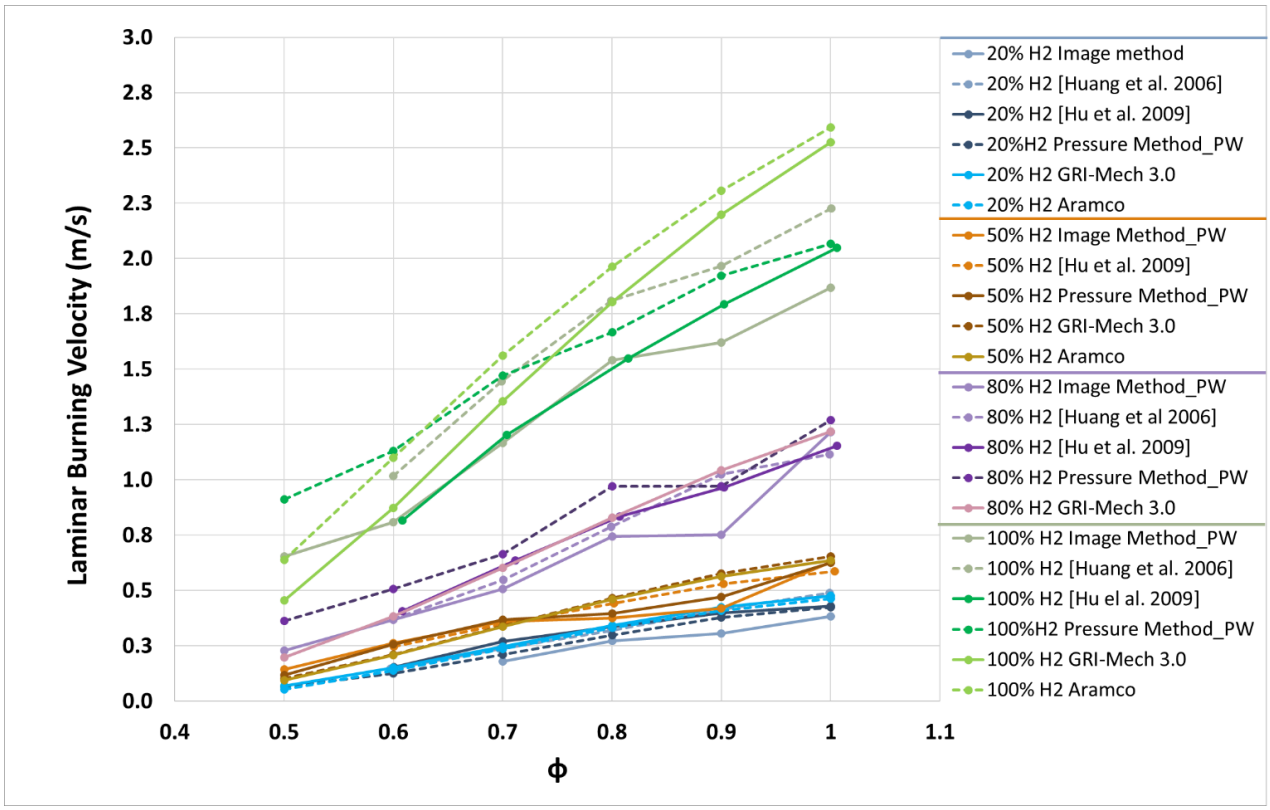

Figure 9. Laminar burning velocity of hydrogen/methane/air mixtures in initial conditions of 0.1 MPa and 300–315 K.

3.3. Flame Morphological Study

In real flames, there are several phenomena that may modify, among other properties, the laminar burning velocity and that can develop instabilities in the flame front, eventually leading to cellular flames. Instabilities formed in the flame front are due to a variety of phenomena that need to be characterized and studied. There are different phenomena in the flame that generate instabilities or perturbations in the flame front, which can cause the flame front to deform and wrinkle. The main phenomena are volume forces, such as gravity, thermal expansion of gases due to the flame front development (hydrodynamics), and phenomena with a thermo-diffusive origin. The effect of the perturbations on the laminar burning velocity is double: firstly, the increase in flame speed due to an increment in the flame front surface; secondly, flame and flow geometry deformations, resulting in changes in velocity magnitude and direction, due to the difference between the mass and thermal diffusivities of the reactants. The deviation of flame sphericity and flux with respect to the one-dimensional flame can be quantified through the strain stretch rate and the curvature of the flame front [42].

In spherical flames, the initial moment of the growth of the perturbations of the flame front does not necessarily have to coincide with the time for which the instability is observed experimentally. This explains why disturbances may not be detected until their amplitude reaches a significant size [55]. The growth rate of the flame front depends on three main factors: thermal, molecular, and viscous diffusivity. The thermal diffusivity has a stabilizing effect of the instabilities due to the variation of temperature. The diffusivity due to the viscosity also has a stabilizing effect, due to the important variation of viscosity across the entire surface of the flame front. The laminar burning velocity obtained in the present work was compared with the results obtained in [20,56–58].

In Figures 10 and 11, images of five different fuel/air mixtures are presented in order to study the effect of hydrogen addition on the instabilities apparition and their effect on the flame front morphology for 1.0 and 0.7 equivalence ratios. The images were captured every 0.01 m (1 cm). Mixtures of 100% CH_4 had a completely laminar flame front. For the mixture of 50% H_2, the flame began to develop small cracks from 3 cm of radius, which led brusquely to a wrinkly flame front (cellularity) at the end of combustion when the flame front was near the pump wall. For the mixtures of 80% and 100% H_2, the flame front developed cells at the early stages of combustion, which grew throughout the process. Images presented in Figures 10 and 11 show the three regimens in the combustion of H_2/CH_4 mixtures explained before. The addition of hydrogen to the fuel/air mixture accelerated the rate of the chemical reactions produced during the combustion and enhanced the instability of the flame. In Figures 10 and 11, it is also possible to see the increment in the flame instability with the increment in the flame radius. As the radius and the hydrogen content increased, the cracks developed in the flame front due to the increment in the hydrodynamic and thermal–diffusive instabilities, while the cellular structure of the flame front also increased.

In Figures 10 and 11, two kinds of flames can be distinguished: blends with less H_2 content and those with more H_2 content. The first group, with dominant methane, had a laminar flame until the end, only affected by a few cracks that did not lead to a cellular front. On the contrary, the second group, with dominant hydrogen, had an instable flame appearance from the beginning and the cracks led to a cellular flame front.

The first behavior was observed for mixtures with low hydrogen content. For example, in the stoichiometric case (Figure 10), the flame was initially stable; only when the hydrogen in the fuel mixture exceeded 50% did cracks and cellularity develop. For lean mixtures (Figure 11), the flame developed wrinkles and cracks with a lower hydrogen content, 20%.

This can be explained as follows: in the initial phase of flame development, flame instability is influenced mainly by the thermo-diffusive effect. However, as the flame develops and the flame radius increases, the hydrodynamic effect becomes the dominant contribution to instability. Hydrodynamic instability depends on the thermal expansion (rate between densities of the unburned and the burned gases); hydrogen slightly reduces the density

ratio, but it does not affect the general behavior of the hydrodynamic instabilities, which always tend to destabilize the flame front.

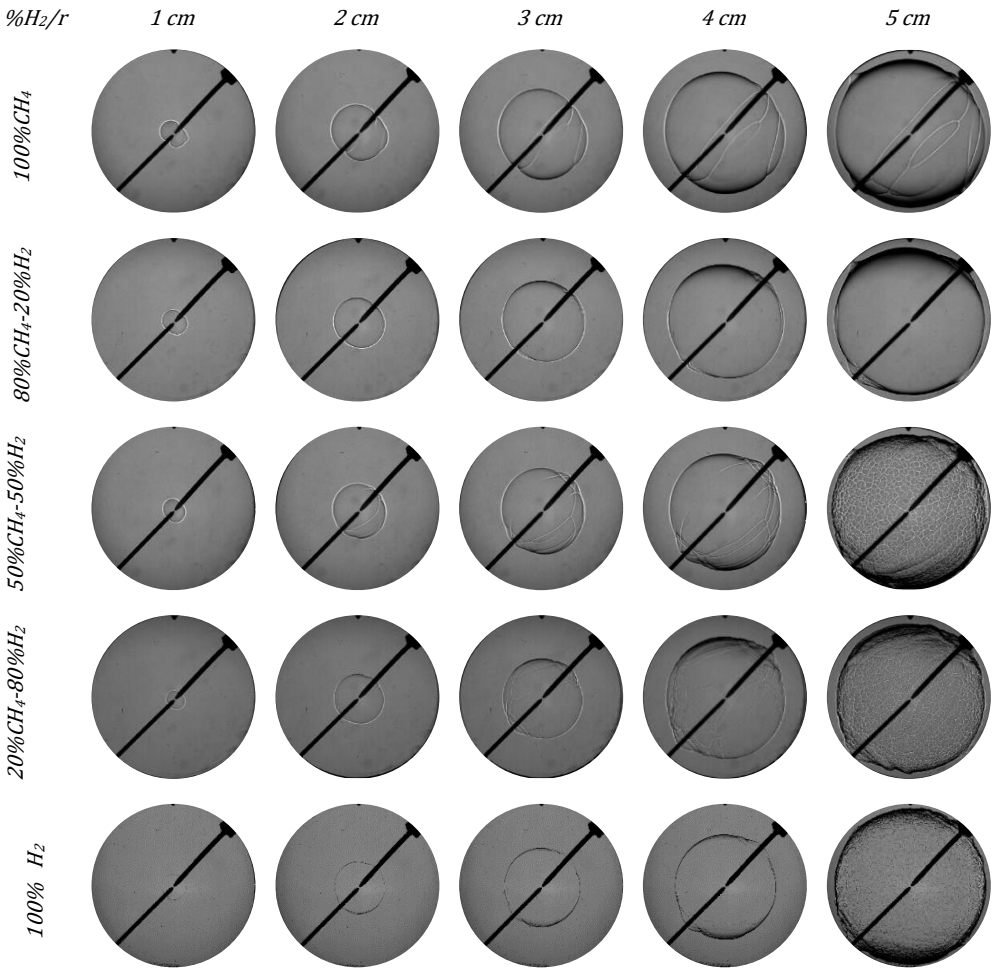

Figure 10. Schlieren images of different H_2/CH_4 mixtures in initial conditions of 0.1 MPa, 315 K, and 1.0 equivalence ratio.

However, thermal–diffusive instability is greatly affected by the hydrogen proportion of the blends, since it mainly depends on the Lewis number, among other parameters. The Lewis number changes according to the chemical and physical properties of the fuel blend, which decrease with hydrogen addition. The value of the Lewis number mostly defines the sign and, therefore, the behavior (flame stabilizing or destabilizing) of the thermal–diffusive instabilities, which ultimately mark the flame morphology.

Hydrogen addition has a greater effect on the thermal–diffusive instability than on the hydrodynamic instability, although it affects both [41].

When Figures 10 and 11 are compared to investigate the effect of the fuel/air equivalence ratio, it is possible to see that flames with lower equivalence ratios showed earlier cracks in the flame front morphology and developed an earlier cellular structure. The structure of the cellular flames under lean conditions was different from that under stoichiometric conditions, due to the different origin of the dominant instabilities. For a stoichiometric fuel/air equivalence ratio, the cellular flames had a defined spherical shape, since there were no big wrinkles on the surface, and the cells (arisen from hydrodynamic instabilities) were homogeneously spread out. However, for lean mixtures (Figure 11), there were large-scale wrinkles (due to thermal–diffusive instabilities) combined with smaller-scale cells, giving a clustered structure aspect to the flame.

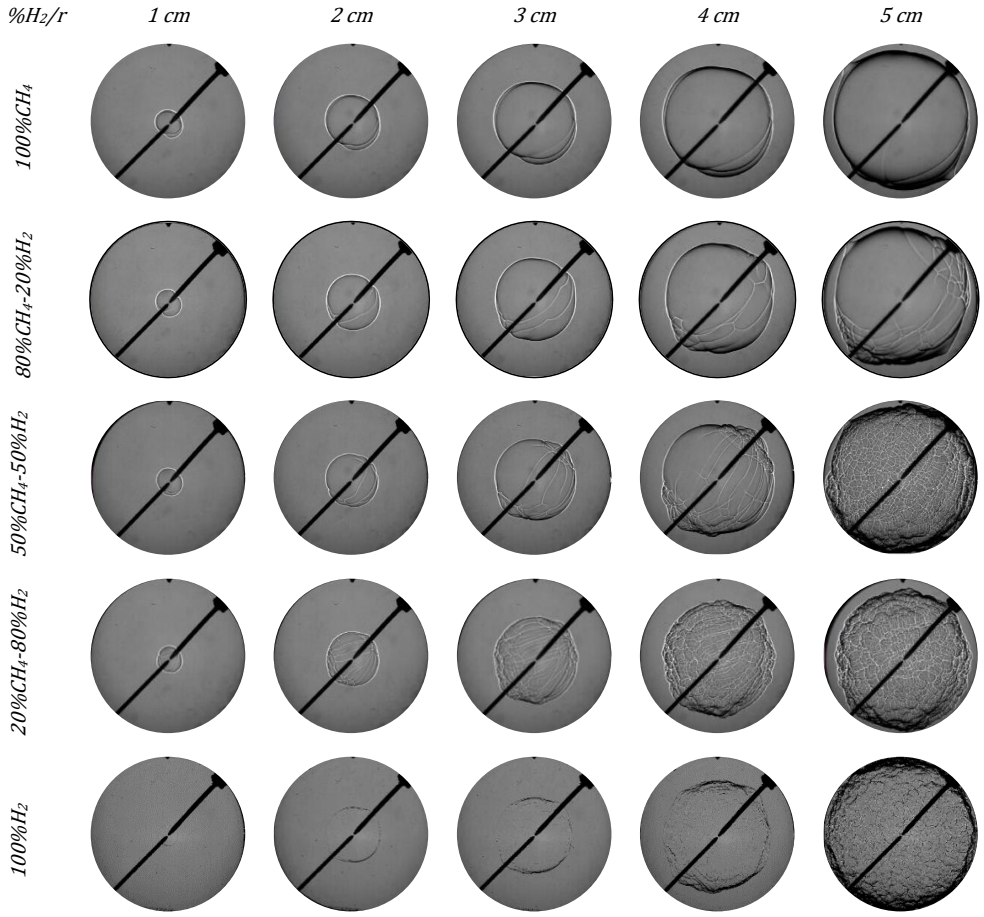

Figure 11. Schlieren images of different H_2/CH_4 mixtures in initial conditions of 0.1 MPa, 300 K, and 0.7 equivalence ratio.

Hydrodynamic instability and thermal–diffusive instability are the main contributions to the cellular structure formation [36,59,60]. The destabilization in hydrogen combustion due to hydrodynamic instability is reflected by the decrement in the flame front thickness (δ) [61], as can be seen in Figure 12, where the effect of the hydrogen content in the fuel/air mixture on the flame front thickness is presented [17]. Khan et al. [48] obtained the same tendency in the variation of calculated laminar flame thickness versus the equivalence ratio, for different hydrogen/methane mixtures.

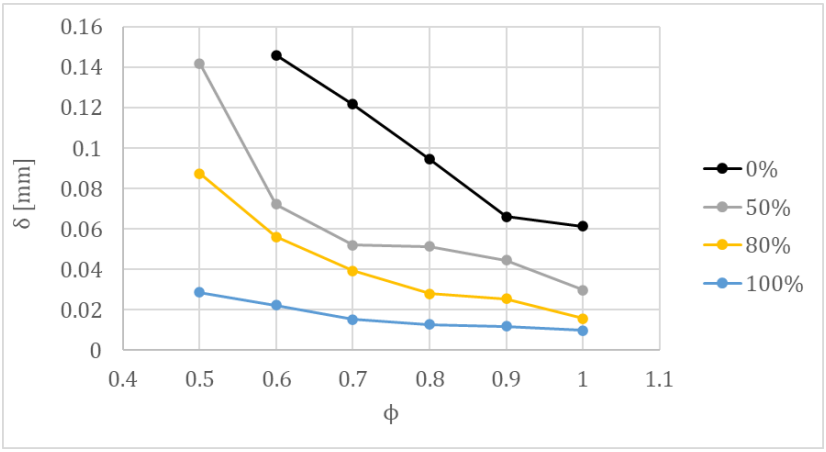

Figure 12. Flame thickness of hydrogen/methane mixtures for different equivalence ratios at 315 K and 0.1 MPa.

3.4. Effect of Hydrogen Content on NOx Emissions

The addition of hydrogen and increment in the fuel/air ratio increased the combustion temperature, as plotted in Figure 13; consequently, NOx emissions increased simultaneously, as presented in a previous study [3] by our research team for percentages of hydrogen in the mixture up to 15%. Law et al. [16] studied hydrogen flames by adding small fractions of hydrocarbon fuels, and they showed a decrease in the laminar burning velocity and flame temperature as the hydrocarbons were added.

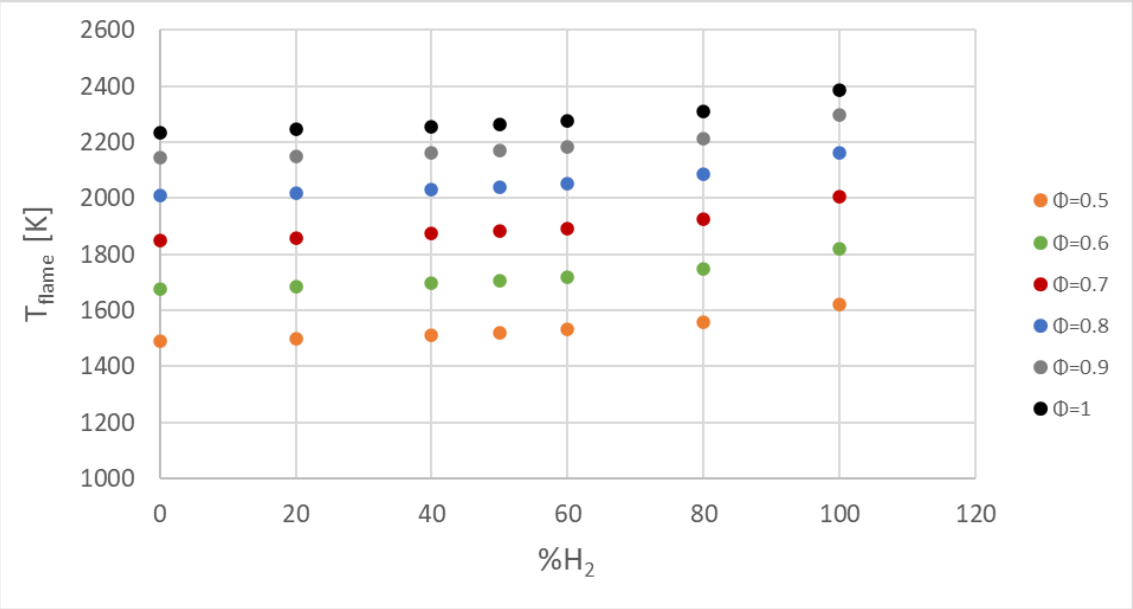

Figure 13. Flame temperature for fuel/air mixtures with different percentages of hydrogen in conditions of 0.1 MPa, 300 K, and equivalence ratios of 0.5–1.

Many researchers obtained the same tendency of NOx emissions with the increment in the hydrogen content in the fuel mixture [62–65]. Figure 14 shows the NOx mole fraction in combustions of hydrogen/methane mixtures for different hydrogen content and fuel/air equivalence ratios. These figures were obtained using the kinetic mechanism for hydrogen/methane combustion developed by Conaire et al. [66] in the Cantera software. The NO values remained nearly constant until the hydrogen content exceeded 60%, at which point the values increased moderately. The same behavior can be observed in Figure 14b with NO_2 emissions, but the increment when hydrogen content exceeded 60% was lower than in the case of NO. The formation mechanisms of NO and NO_2 were detailed in Shudo et al. [67]. This trend differed from that obtained directly in the engine test due to the difference in operating conditions between the combustion bomb and the internal combustion engine. Wang et al. [68] observed that the chemical kinetics of hydrogen addition had little influence on the NO emissions during methane combustion. Naha et al. [69] conducted a numerical investigation of hydrocarbons/hydrogen flames by analyzing NO and CO, among other components. Emissions of C_2H_2 (considered as a soot precursor and important in the formation of prompt NO) were reduced with the addition of hydrogen to methane mixtures, while CO emissions remained unaffected, and NO emissions increased slightly.

CO and CO_2 emissions are presented in Figure 15, where it is possible to see that the increment in the methane content in the fuel/air mixture increased both values, as expected, obtaining a maximum value for the CO_2 emissions near the stoichiometric mixture, while CO increased with the equivalence ratio. This behavior can be attributed to two factors: first, the addition of hydrogen, for the same strain rate, decreased carbon content in the fuel, which reduced the amount of CO; second, hydrogen addition increased the OH radical (in CO oxidation, OH is a dominant radical) and decreased the CO emissions.

The increment in the OH radicals increased the oxidation rates of CO, and then reduced its concentration. Hydrogen addition also decreased the CO_2 emissions by decreasing the net content of carbon in the fuel mixture, as can be seen in Figure 15. In Figure 16, OH radical concentration is presented versus the fuel/air equivalence ratio for different fuel/air mixtures, where it is possible to see an increase in OH radicals with the addition of hydrogen on the fuel mixture. Many other studies [54,70] also obtained an increment in OH radicals as the percentage of hydrogen increased in the fuel mixture. A correlation was observed between laminar burning velocity and maximum OH radical concentrations, with high laminar burning velocity corresponding with high OH concentration.

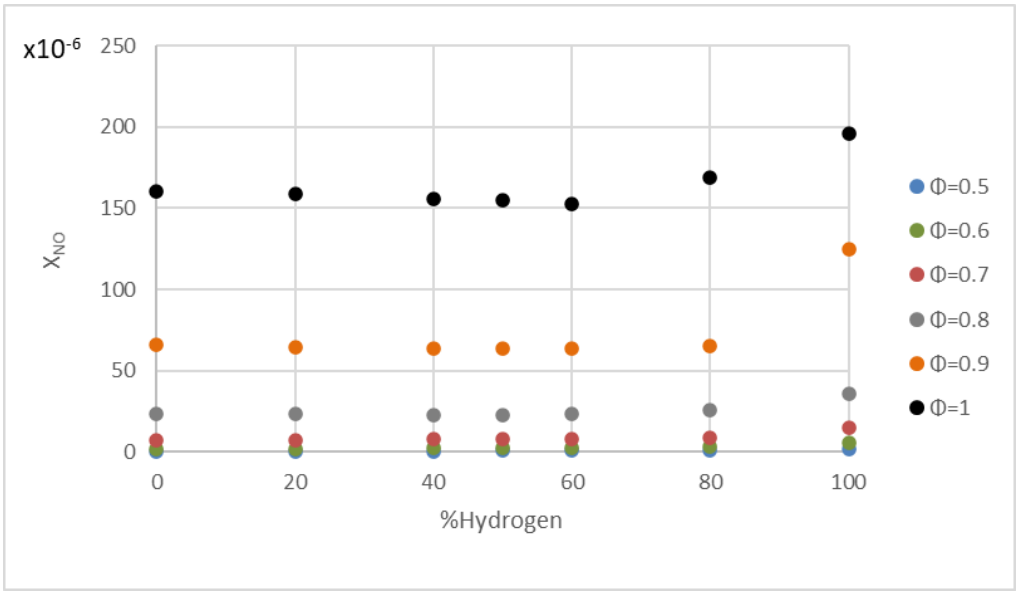

(**a**) NO emissions

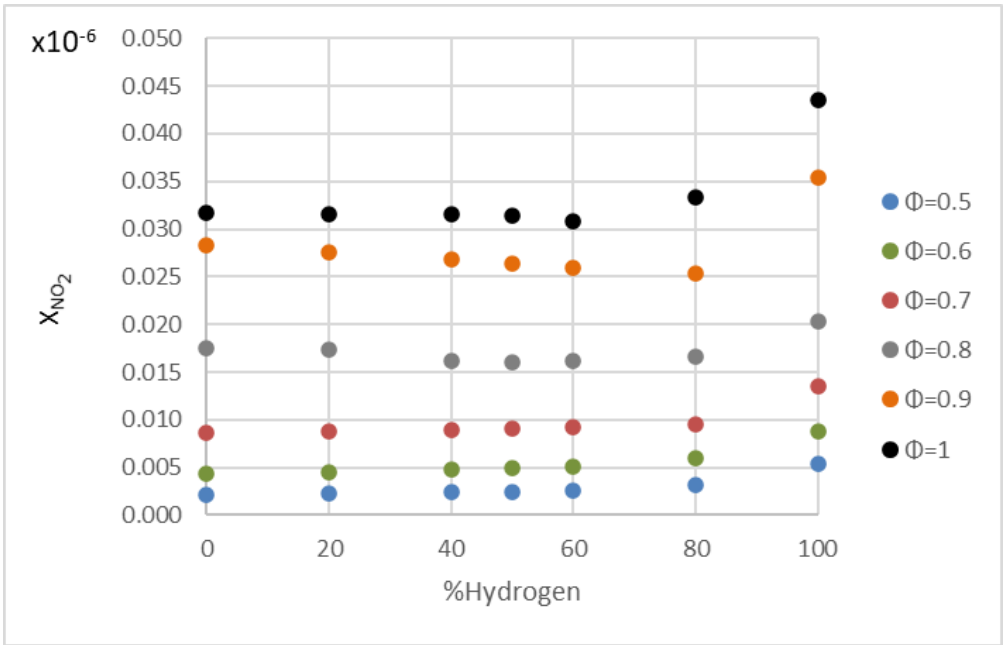

(**b**) NO_2 emissions

Figure 14. NO and NO_2 emissions for fuel/air mixtures with different percentages of hydrogen in conditions of 0.1 MPa, 300 K, and equivalence ratios of 0.5–1.

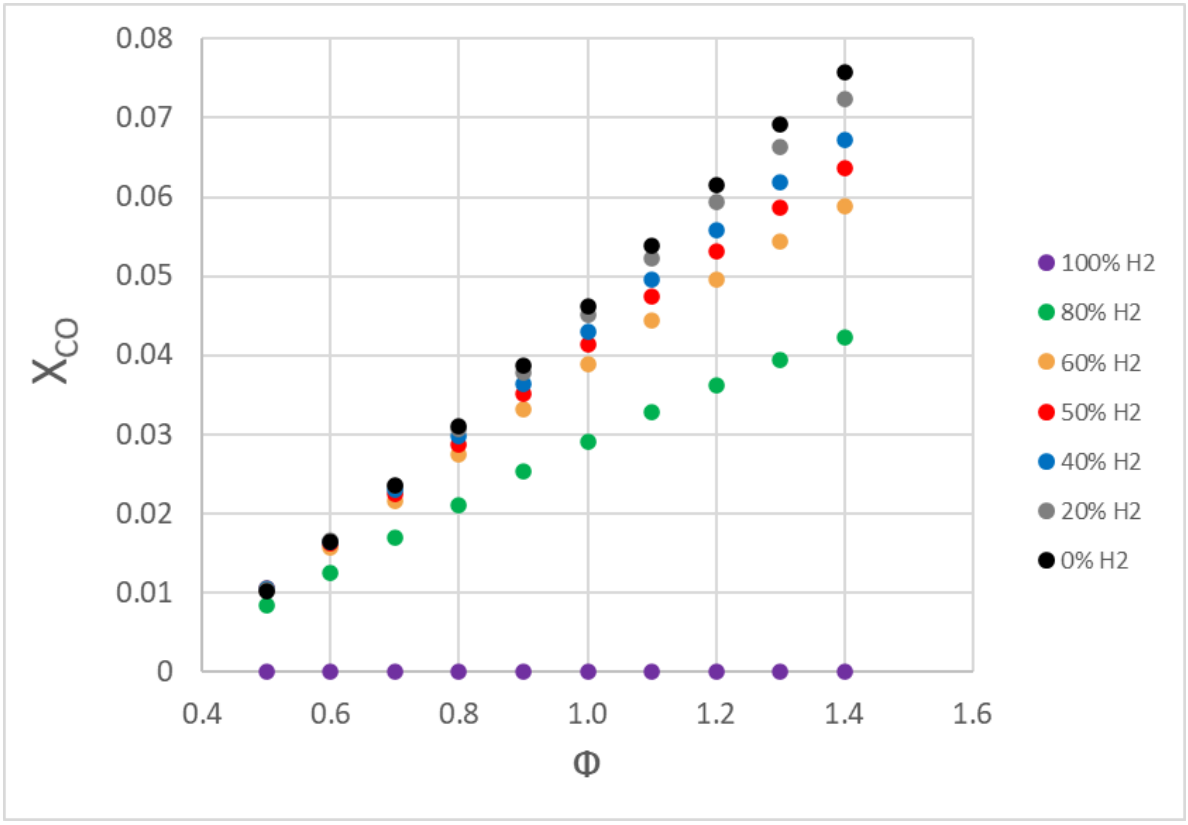

(**a**) CO emissions

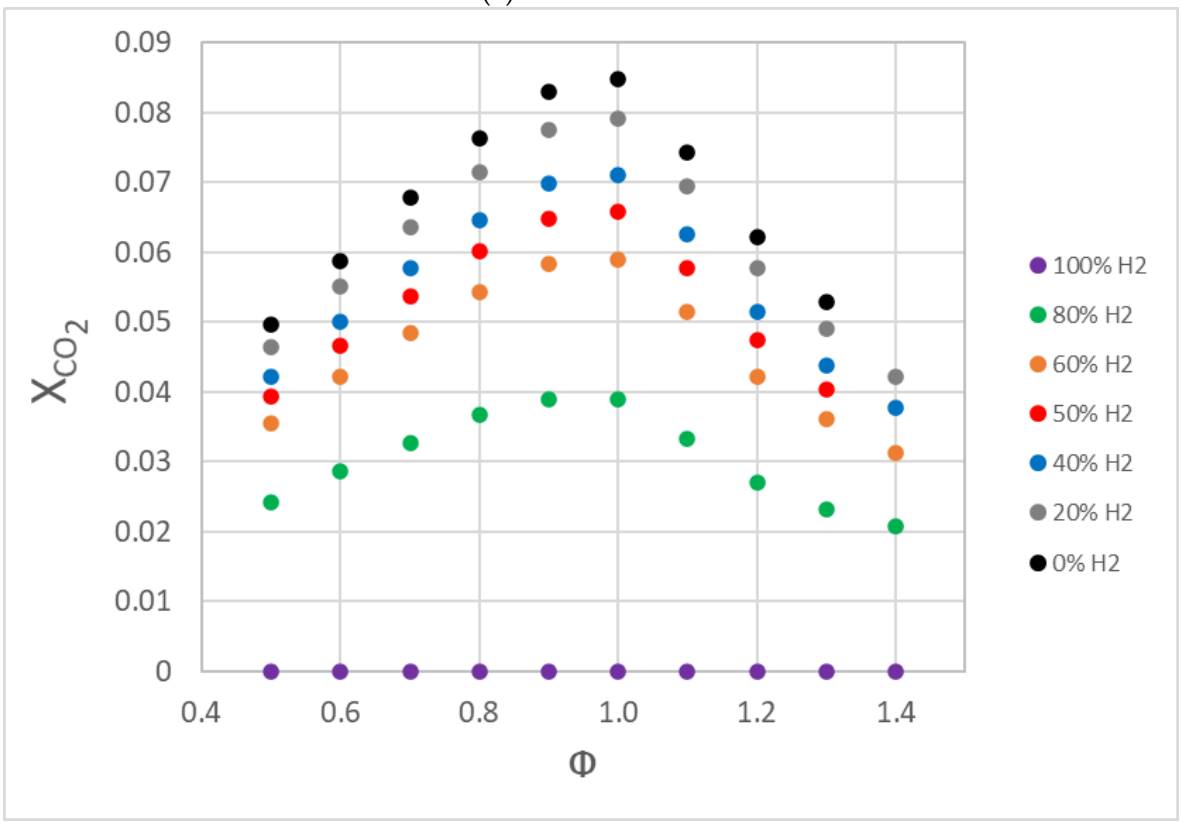

(**b**) CO_2 emissions

Figure 15. CO and CO_2 emissions for fuel/air mixtures with different percentages of hydrogen in conditions of 0.1 MPa, 300 K, and equivalence ratios of 0.5–1.4.

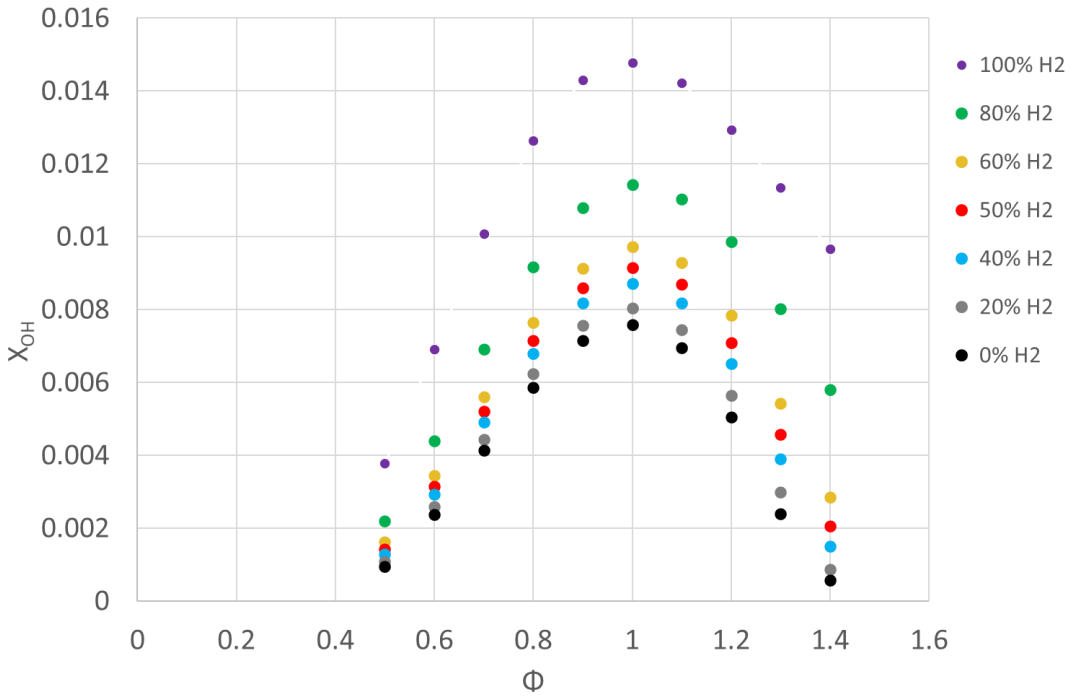

Figure 16. OH radical concentration for fuel/air mixtures with different percentages of hydrogen in conditions of 0.1 MPa, 300 K, and equivalence ratios of 0.5–1.4.

4. Conclusions

Hydrogen content in H_2/CH_4/air mixtures enhances the combustion process and increases the burning velocity. Depending on the fraction of hydrogen added to the fuel mixture, three regimens can be identified: the combustion regime dominated by methane where the hydrogen fraction is less than 40%, the transitional regime with a hydrogen fraction between 50% and 80%, and the hydrogen dominated combustion regime in which the hydrogen fraction is greater than 80%. The increase in flame speed is more affected by the hydrogen content.

The present work showed that the addition of moderate percentages of hydrogen to methane increased its burning velocity and modified the flame morphology, changing the flame front structure from a totally laminar combustion (for methane, with a spherical morphology) to a cellular combustion, with cellularity of the flame front from the start of combustion for lower equivalence ratios (hydrogen), accounting for relevant variables such as the mass and thermal diffusivities of hydrogen and methane.

The hydrogen content in the fuel mixture accelerated the cellularity development, with a greater effect on the thermal–diffusive instability than on the hydrodynamic instability, which produced an increment in the cracks developed in the flame. This transition to cellularity was characterized through the study of the flame instabilities and flame front thickness. Flame instability increased with the increment in the flame radius and with lower fuel/air equivalence ratios in the fuel/air mixture, because the structure of the cellular flames under lean conditions was different from that under stoichiometric conditions due to the different origin of the dominant instabilities.

NOx, CO, and CO_2 emissions were investigated using kinetic modeling, obtaining an increment in NOx emissions with the increment in hydrogen content in the fuel mixture, due to the increment in the flame temperature. However, CO and CO_2 decreased with hydrogen addition to the fuel mixture. The results agree with those obtained in the literature. The addition of hydrogen to the fuel mixture modified the combustion chemistry due to the higher reactivity of H_2 and the higher content of H and OH radicals. The increment in the OH radicals increased the oxidation rate of CO, and then reduced its concentration. The increment in hydrogen content also decreased the CO_2 emissions by reducing the carbon

content in the fuel mixture. However, hydrogen content had a minor effect on NO and NO_2 emissions for percentages of hydrogen lower than 80%. On the other hand, when the percentage of hydrogen in the fuel mixture exceeded 80%, the NO and NO_2 emissions increased significantly.

Author Contributions: Conceptualization, M.R. and B.G.; methodology, M.R. and R.S.; kinetic modeling, C.S.; validation, M.R., R.S. and B.G.; investigation, M.R., C.S. and R.S.; writing—review and editing, M.R. All authors have read and agreed to the published version of the manuscript.

Funding: This research was funded by the Spanish Ministry of Science and Innovation-Agencia Estatal de Investigación research project PID2019-106957RB-C22.

Acknowledgments: The authors would like to thank the Spanish Ministry of Science and Innovation-Agencia Estatal de Investigación for the financial support of this investigation through the research project PID2019-106957RB-C22. This work was developed under the support of the Research Group in Engines and Renewable Energies (MyER) from the University of Valladolid.

Conflicts of Interest: The authors declare no conflict of interest.

References

1. Ravi, K.; Mathew, S.; Bhasker, J.P.; Porpatham, E. Gaseous alternative fuels for Spark Ignition Engines—A technical review. *J. Chem. Pharm. Sci.* **2017**, *10*, 93–99.
2. Reyes, M.; Melgar, A.; Pérez, A.; Giménez, B. Study of the cycle-to-cycle variations of an internal combustion engine fuelled with natural gas/hydrogen blends from the diagnosis of combustion pressure. *Int. J. Hydrogen Energy* **2013**, *38*, 15477–15487. [CrossRef]
3. Tinaut, F.; Melgar, A.; Gimenez, B.; Reyes, M. Prediction of performance and emissions of an engine fuelled with natural gas/hydrogen blends. *Int. J. Hydrogen Energy* **2011**, *36*, 947–956. [CrossRef]
4. Gu, X.J.; Haq, M.Z.; Lawes, M.; Woolley, R. Laminar burning velocity and Markstein lengths of methane-air mixtures. *Combust. Flame* **2000**, *121*, 41–58. [CrossRef]
5. Liao, S.; Jiang, D.; Gao, J.; Huang, Z. Measurements of Markstein numbers and laminar burning velocities for natural gas-air mixtures. *Energy Fuels* **2004**, *18*, 316–326. [CrossRef]
6. Karlovitz, B.; Denniston, D., Jr.; Knapschaefer, D.; Wells, F. *Studies on Turbulent Flames: A. Flame Propagation Across Velocity Gradients B. Turbulence Measurement in Flames, Proceedings of the Symposium (International) on Combustion, Cambridge, MA, USA, 1–5 September 1952*; Elsevier: Amsterdam, The Netherlands, 1953; pp. 613–620.
7. Yu, G.; Law, C.; Wu, C. Laminar flame speeds of hydrocarbon+ air mixtures with hydrogen addition. *Combust. Flame* **1986**, *63*, 339–347. [CrossRef]
8. Tseng, L.-K.; Ismail, M.; Faeth, G.M. Laminar burning velocities and Markstein numbers of hydrocarbonair flames. *Combust. Flame* **1993**, *95*, 410–426. [CrossRef]
9. Reyes, M.; Tinaut, F.V.; Horrillo, A.; Lafuente, A. Experimental characterization of burning velocities of premixed methane-air and hydrogen-air mixtures in a constant volume combustion bomb at moderate pressure and temperature. *Appl. Therm. Eng.* **2018**, *130*, 684–697. [CrossRef]
10. Naber, J.; Siebers, D.; Di Julio, S.; Westbrook, C. Effects of natural gas composition on ignition delay under diesel conditions. *Combust. Flame* **1994**, *99*, 192–200. [CrossRef]
11. Sun, C.; Sung, C.-J.; He, L.; Law, C.K. Dynamics of weakly stretched flames: Quantitative description and extraction of global flame parameters. *Combust. Flame* **1999**, *118*, 108–128. [CrossRef]
12. Hermanns, R.; Konnov, A.; Bastiaans, R.; De Goey, L. Laminar burning velocities of diluted hydrogen-oxygen-nitrogen mixtures. *Energy Fuels* **2007**, *21*, 1977–1981. [CrossRef]
13. Qiao, L.; Kim, C.; Faeth, G. Suppression effects of diluents on laminar premixed hydrogen/oxygen/nitrogen flames. *Combust. Flame* **2005**, *143*, 79–96. [CrossRef]
14. Reyes, M.; Tinaut, F.V. Characterization of the burning velocity of hydrogen/methane blends in a constant volume combustion bomb. In Proceedings of the 2017 8th International Conference on Mechanical and Aerospace Engineering, ICMAE 2017, Prague, Czech Republic, 22–25 July 2017; pp. 257–261.
15. Milton, B.E.; Keck, J.C. Laminar burning velocities in stoichiometric hydrogen and hydrogen-hydrocarbon gas mixtures. *Combust. Flame* **1984**, *58*, 13–22. [CrossRef]
16. Law, C.K.; Kwon, O. Effects of hydrocarbon substitution on atmospheric hydrogen–air flame propagation. *Int. J. Hydrogen Energy* **2004**, *29*, 867–879. [CrossRef]
17. Halter, F.; Chauveau, C.; Djebaïli-Chaumeix, N.; Gökalp, I. Characterization of the effects of pressure and hydrogen concentration on laminar burning velocities of methane-hydrogen-air mixtures. *Proc. Combust. Inst.* **2005**, *30*, 201–208. [CrossRef]
18. Scholte, T.; Vaags, P. Burning velocities of mixtures of hydrogen, carbon monoxide and methane with air. *Combust. Flame* **1959**, *3*, 511–524. [CrossRef]

19. Liu, Y.; Lenze, B. Investigation of flame-generated turbulence in premixed flames at low and high burning velocities. *Exp. Therm. Fluid Sci.* **1992**, *5*, 410–415. [CrossRef]
20. Huang, Z.; Zhang, Y.; Zeng, K.; Liu, B.; Wang, Q.; Jiang, D. Measurements of laminar burning velocities for natural gas-hydrogen-air mixtures. *Combust. Flame* **2006**, *146*, 302–311. [CrossRef]
21. Fairweather, M.; Ormsby, M.P.; Sheppard, C.G.W.; Woolley, R. Turbulent burning rates of methane and methane-hydrogen mixtures. *Combust. Flame* **2009**, *156*, 780–790. [CrossRef]
22. Ji, C.; Wang, D.; Yang, J.; Wang, S. A comprehensive study of light hydrocarbon mechanisms performance in predicting methane/hydrogen/air laminar burning velocities. *Int. J. Hydrogen Energy* **2017**, *42*, 17260–17274. [CrossRef]
23. Sun, Z.-Y.; Li, G.-X. Propagation characteristics of laminar spherical flames within homogeneous hydrogen-air mixtures. *Energy* **2016**, *116*, 116–127. [CrossRef]
24. Tinaut, F.; Reyes, M.; Melgar, A.; Giménez, B. Optical characterization of hydrogen-air laminar combustion under cellularity conditions. *Int. J. Hydrogen Energy* **2019**, *44*, 12857–12871. [CrossRef]
25. Sun, Z.-Y.; Li, G.-X.; Li, H.-M.; Zhai, Y.; Zhou, Z.-H. Buoyant unstable behavior of initially spherical lean hydrogen-air premixed flames. *Energies* **2014**, *7*, 4938–4956. [CrossRef]
26. Williams, F.A. *Combustion Theory*; CRC Press: Boca Raton, FL, USA, 1985.
27. Matalon, M.; Matkowsky, B.J. Flames as gasdynamic discontinuities. *J. Fluid Mech.* **1982**, *124*, 239–259. [CrossRef]
28. Addabbo, R.; Bechtold, J.; Matalon, M. Wrinkling of spherically expanding flames. *Proc. Combust. Inst.* **2002**, *29*, 1527–1535. [CrossRef]
29. Askari, O.; Wang, Z.; Vien, K.; Sirio, M.; Metghalchi, H. On the flame stability and laminar burning speeds of syngas/O_2/He premixed flame. *Fuel* **2017**, *190*, 90–103. [CrossRef]
30. Altantzis, C.; Frouzakis, C.E.; Tomboulides, A.G.; Matalon, M.; Boulouchos, K. Hydrodynamic and thermodiffusive instability effects on the evolution of laminar planar lean premixed hydrogen flames. *J. Fluid Mech.* **2012**, *700*, 329–361. [CrossRef]
31. Hao, D.; Mehra, R.K.; Luo, S.; Nie, Z.; Ren, X.; Fanhua, M. Experimental study of hydrogen enriched compressed natural gas (HCNG) engine and application of support vector machine (SVM) on prediction of engine performance at specific condition. *Int. J. Hydrogen Energy* **2020**, *45*, 5309–5325. [CrossRef]
32. Sagar, S.; Agarwal, A.K. Knocking behavior and emission characteristics of a port fuel injected hydrogen enriched compressed natural gas fueled spark ignition engine. *Appl. Therm. Eng.* **2018**, *141*, 42–50. [CrossRef]
33. Tangöz, S.; Kahraman, N.; Akansu, S.O. The effect of hydrogen on the performance and emissions of an SI engine having a high compression ratio fuelled by compressed natural gas. *Int. J. Hydrogen Energy* **2017**, *42*, 25766–25780. [CrossRef]
34. Tinaut, F.; Melgar, A.; Horrillo, A. *Utilization of a Quasi-Dimensional Model for Predicting Pollutant Emissions in SI Engines*; SAE Technical Paper 1999-01-0223; SAE International: Warrendale, PA, USA, 1999. [CrossRef]
35. Tinaut, F.V.; Reyes, M.; Giménez, B.; Pastor, J.V. Measurements of OH* and CH* Chemiluminescence in Premixed Flames in a Constant Volume Combustion Bomb under Autoignition Conditions. *Energy Fuels* **2011**, *25*, 119–129. [CrossRef]
36. Jiang, Y.-H.; Li, G.-X.; Li, F.-S.; Sun, Z.-Y.; Li, H.-M. Experimental investigation of correlation between cellular structure of the flame front and pressure. *Fuel* **2017**, *199*, 65–75. [CrossRef]
37. Kim, W.; Sato, Y.; Johzaki, T.; Endo, T. Experimental study on the onset of flame acceleration due to cellular instabilities. *J. Loss Prev. Process Ind.* **2019**, *60*, 264–268. [CrossRef]
38. Wu, F.; Jomaas, G.; Law, C.K. An experimental investigation on self-acceleration of cellular spherical flames. *Proc. Combust. Inst.* **2013**, *34*, 937–945. [CrossRef]
39. Di Sarli, V.; Benedetto, A.D. Laminar burning velocity of hydrogen-methane/air premixed flames. *Int. J. Hydrogen Energy* **2007**, *32*, 637–646. [CrossRef]
40. El-Sherif, S. Control of emissions by gaseous additives in methane-air and carbon monoxide-air flames. *Fuel* **2000**, *79*, 567–575. [CrossRef]
41. Reyes, M.; Tinaut, F.V.; Giménez, B.; Camaño, A. Combustion and Flame Front Morphology Characterization of H2–CO Syngas Blends in Constant Volume Combustion Bombs. *Energy Fuels* **2021**, *35*, 3497–3511. [CrossRef]
42. Bradley, D.; Gaskell, P.; Gu, X. Burning velocities, Markstein lengths, and flame quenching for spherical methane-air flames: A computational study. *Combust. Flame* **1996**, *104*, 176–198. [CrossRef]
43. Okafor, E.C.; Nagano, Y.; Kitagawa, T. Experimental and theoretical analysis of cellular instability in lean H2-CH4-air flames at elevated pressures. *Int. J. Hydrogen Energy* **2016**, *41*, 6581–6592. [CrossRef]
44. Clavin, P.; Williams, F. Effects of molecular diffusion and of thermal expansion on the structure and dynamics of premixed flames in turbulent flows of large scale and low intensity. *J. Fluid Mech.* **1982**, *116*, 251–282. [CrossRef]
45. Goodwin, D.G.; Moffat, H.K.; Speth, R.L. *Cantera: An Object-Oriented Software Toolkit for Chemical Kinetics, Thermodynamics, and Transport Processes*; Caltech: Pasadena, CA, USA, 2009; Volume 124.
46. Gregory, P.; Golden, D.; Frenklach, M.; Moriarty, N.; Eiteneer, B.; Goldenberg, M.; Qin, Z. *GRI-Mech 3.0 (Tech. Rep.)*; UC Berkeley: Berkeley, CA, USA, 2018.
47. Hermanns, R.T.E.; Kortendijk, J.; Bastiaans, R.; De Goey, L. Laminar burning velocities of methane-hydrogen-air mixtures. *Submitt. Combust. Flame* **2007**. Available online: https://www.researchgate.net/publication/268807456 (accessed on 24 April 2022).
48. Khan, A.; Ravi, M.; Ray, A. Experimental and chemical kinetic studies of the effect of H2 enrichment on the laminar burning velocity and flame stability of various multicomponent natural gas blends. *Int. J. Hydrogen Energy* **2019**, *44*, 1192–1212. [CrossRef]

49. Wang, T.; Zhang, X.; Zhang, J.; Hou, X. Automatic generation of a kinetic skeletal mechanism for methane-hydrogen blends with nitrogen chemistry. *Int. J. Hydrogen Energy* **2018**, *43*, 3330–3341. [CrossRef]
50. Li, R.; Luo, Z.; Wang, T.; Cheng, F.; Lin, H.; Zhu, X. Effect of initial temperature and H2 addition on explosion characteristics of H2-poor/CH4/air mixtures. *Energy* **2020**, *213*, 118979. [CrossRef]
51. Nilsson, E.J.; van Sprang, A.; Larfeldt, J.; Konnov, A.A. The comparative and combined effects of hydrogen addition on the laminar burning velocities of methane and its blends with ethane and propane. *Fuel* **2017**, *189*, 369–376. [CrossRef]
52. Hu, E.; Li, X.; Meng, X.; Chen, Y.; Cheng, Y.; Xie, Y.; Huang, Z. Laminar flame speeds and ignition delay times of methane-air mixtures at elevated temperatures and pressures. *Fuel* **2015**, *158*, 1–10. [CrossRef]
53. Konnov, A.A.; Mohammad, A.; Kishore, V.R.; Kim, N.I.; Prathap, C.; Kumar, S. A comprehensive review of measurements and data analysis of laminar burning velocities for various fuel+ air mixtures. *Prog. Energy Combust. Sci.* **2018**, *68*, 197–267. [CrossRef]
54. Hu, E.; Huang, Z.; He, J.; Miao, H. Experimental and numerical study on lean premixed methane-hydrogen-air flames at elevated pressures and temperatures. *Int. J. Hydrogen Energy* **2009**, *34*, 6951–6960. [CrossRef]
55. Reyes, M.; Sastre, R.; Tinaut, F.V.; Rodríguez-Fernández, J. Study and characterization of the instabilities generated in expanding spherical flames of hydrogen/methane/air mixtures. *Int. J. Hydrogen Energy* **2022**.
56. Bougrine, S.; Richard, S.; Nicolle, A.; Veynante, D. Numerical study of laminar flame properties of diluted methane-hydrogen-air flames at high pressure and temperature using detailed chemistry. *Int. J. Hydrogen Energy* **2011**, *36*, 12035–12047. [CrossRef]
57. Coppens, F.; De Ruyck, J.; Konnov, A.A. Effects of hydrogen enrichment on adiabatic burning velocity and NO formation in methane+ air flames. *Exp. Therm. Fluid Sci.* **2007**, *31*, 437–444. [CrossRef]
58. Tanoue, K.; Goto, S.; Shimada, F.; Hamatake, T. Effects of hydrogen addition on stretched premixed laminar methane flames (1st report, effects on laminar burning velocity). *Trans Jpn. Soc Mech Eng B* **2003**, *69*, 162–168. [CrossRef]
59. Jiang, Y.-H.; Li, G.-X.; Li, H.-M.; Li, L.; Tian, L.-L. Study on the influence of flame inherent instabilities on crack propagation of expanding premixed flame. *Fuel* **2018**, *233*, 504–512. [CrossRef]
60. Li, Y.; Jiang, Y.; Xu, W.; Liew, K. Laminar burning velocity and cellular instability of 2-butanone-air flames at elevated pressures. *Fuel* **2022**, *316*, 123390. [CrossRef]
61. Miao, H.; Jiao, Q.; Huang, Z.; Jiang, D. Effect of initial pressure on laminar combustion characteristics of hydrogen enriched natural gas. *Int. J. Hydrogen Energy* **2008**, *33*, 3876–3885. [CrossRef]
62. Ma, F.; Wang, Y.; Liu, H.; Li, Y.; Wang, J.; Zhao, S. Experimental study on thermal efficiency and emission characteristics of a lean burn hydrogen enriched natural gas engine. *Int. J. Hydrogen Energy* **2007**, *32*, 5067–5075. [CrossRef]
63. Choudhuri, A.R.; Gollahalli, S. Combustion characteristics of hydrogen-hydrocarbon hybrid fuels. *Int. J. Hydrogen Energy* **2000**, *25*, 451–462. [CrossRef]
64. Guo, H.; Smallwood, G.J.; Liu, F.; Ju, Y.; Gülder, Ö.L. The effect of hydrogen addition on flammability limit and NOx emission in ultra-lean counterflow CH4/air premixed flames. *Proc. Combust. Inst.* **2005**, *30*, 303–311. [CrossRef]
65. Wang, J.; Huang, Z.; Fang, Y.; Liu, B.; Zeng, K.; Miao, H.; Jiang, D. Combustion behaviors of a direct-injection engine operating on various fractions of natural gas-hydrogen blends. *Int. J. Hydrogen Energy* **2007**, *32*, 3555–3564. [CrossRef]
66. Ó Conaire, M.; Curran, H.J.; Simmie, J.M.; Pitz, W.J.; Westbrook, C.K. A comprehensive modeling study of hydrogen oxidation. *Int. J. Chem. Kinet.* **2004**, *36*, 603–622. [CrossRef]
67. Shudo, T.; Omori, K.; Hiyama, O. NOx reduction and NO2 emission characteristics in rich-lean combustion of hydrogen. *Int. J. Hydrogen Energy* **2008**, *33*, 4689–4693. [CrossRef]
68. Wang, J.; Huang, Z.; Tang, C.; Miao, H.; Wang, X. Numerical study of the effect of hydrogen addition on methane-air mixtures combustion. *Int. J. Hydrogen Energy* **2009**, *34*, 1084–1096. [CrossRef]
69. Naha, S.; Briones, A.M.; Aggarwal, S.K. Effect of fuel blends on pollutant emissions in flames. *Combust. Sci. Technol.* **2004**, *177*, 183–220. [CrossRef]
70. Reyes, M.; Tinaut, F.V.; Giménez, B.; Pastor, J.V. Effect of hydrogen addition on the OH* and CH* chemiluminescence emissions of premixed combustion of methane-air mixtures. *Int. J. Hydrogen Energy* **2018**, *43*, 19778–19791. [CrossRef]